ELSEVIER

International Journal of Mass Spectrometry 219 (2002) 593–613

International Journal of Mass Spectrometry

www.elsevier.com/locate/ijms

Structures, thermochemistry, and infrared spectra of chloride ion–fluorinated acetone complexes and neutral fluorinated acetones in the gas phase: experiment and theory

B. Bogdanov, T.B. McMahon*

Department of Chemistry, University of Waterloo, Waterloo, Ont., Canada N2L 3G1

Received 11 February 2002; accepted 13 May 2002

Dedicated to Yannik Hoppilliard, a gifted scientist and wonderful friend, on the occasion of her 60th birthday.

Abstract

The thermochemistry of chloride ion clustering onto acetone and four fluorinated acetones ($CH_3C(O)CH_2F$, $CF_3C(O)CH_3$, $CF_3C(O)CF_2H$, and $CF_3C(O)CF_3$) under thermal equilibrium conditions has been determined by pulsed-ionization high pressure mass spectrometry (PHPMS). The standard enthalpy (ΔH°) and entropy (ΔS°) changes obtained indicate a variety of different types of bonding in these complexes. Ab initio computational methods have been used to obtain more insight into the structures and energetics. Surprisingly, in the $Cl^-(CF_3C(O)CF_2H)$ complex the chloride ion is not linearly hydrogen bonded, despite the presence of a very acidic CF_2–H bond. Instead, coordination with the carbonyl group carbon atom seems to be more pronounced, as found for the $Cl^-(CF_3C(O)CF_3)$ complex. For the $Cl^-(CF_3C(O)CF_3)$ clustering equilibrium a ΔS° value of $-37.6\,\mathrm{cal\,mol^{-1}\,K^{-1}}$ has been measured, indicating that one or both CF_3 group rotations will be hindered upon complex formation. Excellent agreement between ΔH°_{298} values calculated at the MP2/[6-311++G(3df,3pd)/6-311+G(2df,p)]//MP2/[6-31+G(d)/6-31G(d)] level of theory and experimental ΔH° values has been obtained. In addition, $\Delta_{acid}H^\circ_{298}$ values for a set of small to medium sized organic and inorganic acids, and the fluorinated acetones have been determined at the G3 and G3(MP2) levels of theory. Good to excellent agreement was obtained compared to experimental data, indicating that these composite methods perform well for the determination of reliable $\Delta_{acid}H^\circ_{298}$ results for medium sized molecules containing up to eight second row atoms. No linear correlation between clustering ΔH°_{298} and $\Delta_{acid}H^\circ_{298}$ values was found, indicating that most likely ion–dipole and ion-induced dipole interactions are determining the observed thermochemical trends. Finally, gas phase FT-IR spectra of $CH_3C(O)CH_2F$, $CF_3C(O)CH_3$, $CF_3C(O)CF_2H$, and $CF_3C(O)CF_3$ have been obtained, and the normal mode vibrational frequencies compared to results from calculations at the HF/6-31G(d) level of theory, scaled by 0.8953, and the B3LYP/6-311++G(3d,3p) level of theory. For the $Cl^-(CF_3C(O)CF_3)$ complex some large shifts in frequencies and IR absorption intensities are observed relative to $CF_3C(O)CF_3$, especially for the CO stretch. (Int J Mass Spectrom 219 (2002) 593–613)

Keywords: High pressure mass spectrometry; Ab initio calculations; Thermochemistry of chloride ion–fluorinated acetone complexes; IR spectra of chloride ion–fluorinated acetone complexes

1. Introduction

Multiple interactions or chelation in gas phase ions have been studied extensively, most notably

* Corresponding author. E-mail: mcmahon@uwaterloo.ca

1387-3806/02/$ – see front matter © 2002 Published by Elsevier Science B.V.
PII S1387-3806(02)00745-5

in metal ion–crown ether complexes [1–6]. Less attention has been paid to negatively charged counterparts, where hydrogen bonding may be important [7,8]. Recently, we have reported the structures of chloride ion–ether complexes, and the thermochemistry of their formation [9]. By introducing fluorine atoms, the bonding characteristics and corresponding thermochemistry showed substantial variation. Excellent agreement between experimental and computational results was obtained for most systems, except for the standard entropy change for the formation of the $Cl^-(CF_2HOCF_2H)$ complex. In this complex, the chloride ion interacts with both hydrogen atoms, thereby hindering rotation of both CF_2H groups, and consequently giving rise to a ΔS° value of $-31.3\,\mathrm{cal\,mol^{-1}\,K^{-1}}$. A logical next step to extend this kind of work would be to replace the ether function by a carbonyl function. Larson and McMahon also measured the ΔG°_{298} values for several fluoroacetones (Eq. (1)) using ion cyclotron resonance (ICR) techniques [10].

$$Cl^- + C_3H_nF_{6-n}O \leftrightarrows Cl^-(C_3H_nF_{6-n}O) \qquad (1)$$

Since measurements were confined to a single temperature, no structural deductions based on standard entropy changes, ΔS°, could be made. In the present work, the clustering of chloride ion onto various fluorinated acetones has been investigated using pulsed-ionization high pressure mass spectrometry (PHPMS) and high level ab initio and DFT computational methods. The main objectives were to see the effects of changing the ether linkage to a carbonyl group on the structures and thermochemistry, and to test if the computational method, that was so successful for the chloride ion–ether complexes, is also suitable for the chloride ion–acetone complexes. The computations were also performed to see the effect of chloride ion complex formation on the frequencies and IR intensities of the neutral hexafluoro acetone. In addition, the standard ambient deprotonation enthalpy changes for the fluorinated acetones, $\Delta_{acid}H^\circ_{298}$, were determined at the G3(MP2) level of theory [11]. This was done to test the suitability of this relatively new composite method to obtain thermochemical data, and to obtain more insight into the intrinsic factors that determine the types of binding and the various contributions in these kinds of gas phase cluster ions. Finally, the gas phase FT-IR spectra of $CF_3C(O)CH_2F$, $CF_3C(O)CH_3$, $CF_3C(O)CF_2H$, and $CF_3C(O)CF_3$ were recorded. This was done to test the quality of the calculations and because, surprisingly, no IR spectra of $CF_3C(O)CH_2F$ and $CF_3C(O)CF_2H$ were available in the NIST/EPA Gas-Phase Infrared Database [12].

2. Experimental

2.1. Pulsed-ionization high pressure mass spectrometry

All measurements were carried out on a pulsed-ionization high pressure mass spectrometer (PHPMS), configured around a VG 8-80 mass spectrometer. The instrument, constructed at the University of Waterloo, has been described in detail previously [13]. The general principles and capabilities, as well as the limitations of PHPMS have been described in the literature [14,15].

Gas mixtures were prepared in a 5 L heated stainless steel reservoir at 370 K, by using methane as a bath gas at pressures of 600–800 Torr. Chloride ion was generated from trace amounts of carbon tetrachloride by dissociative electron capture (DEC) of thermalized electrons from 500 μs pulses of a 2 keV electron gun beam.

The five acetones ($CH_3C(O)CH_3$, $CH_3C(O)CH_2F$, $CF_3C(O)CH_3$, $CF_3C(O)CF_2H$, and $CF_3C(O)CF_3$) were added to give relative partial pressures between 0.05 and 5.5%, depending upon the ion source temperature and the nature of the experiment involved. The ion source pressure and temperature ranged from 4.0 to 6.5 Torr and 300 to 550 K, respectively.

Profiles of mass selected ion intensities as a function of reaction time were monitored by using a PC-based multichannel scalar (MCS) data system, configured between 50 and 200 μs dwell time per channel, over 250 channels. Additive accumulations of ion signals resulting from 1000 to 2000 electron gun beam pulses were typically used.

Equilibrium constants (K_{eq}) at different absolute temperatures for the various chloride ion–acetone clustering equilibria (Eq. (1)), are determined from Eq. (2).

$$K_{eq} = \frac{\text{Int}(\text{Cl}^-(\text{C}_3\text{H}_n\text{F}_{6-n}\text{O}))}{\text{Int}(\text{Cl}^-)} \frac{P^0}{P} \quad (2)$$

In Eq. (2), $\text{Int}(\text{Cl}^-(\text{C}_3\text{H}_n\text{F}_{6-n}\text{O}))/\text{Int}(\text{Cl}^-)$ is the ion intensity ratio of the $\text{Cl}^-(\text{C}_3\text{H}_n\text{F}_{6-n}\text{O})$ and Cl^- ions at equilibrium, P^0 is the standard pressure (1 atm), and P is the partial pressure (in atm) of the fluorinated acetone in the ion source.

From the equilibrium constants, the standard Gibbs' free energy change (ΔG°) at different absolute temperatures (T) can be calculated from Eq. (3).

$$\Delta G^\circ = -RT \ln(K_{eq}) \quad (3)$$

By combining Eqs. (3) and (4), the Van't Hoff equation, Eq. (5) can be obtained.

$$\Delta G^\circ = \Delta H^\circ - T\,\Delta S^\circ \quad (4)$$

$$\ln(K_{eq}) = \frac{\Delta S^\circ}{R} - \frac{\Delta H^\circ}{R} \frac{1}{T} \quad (5)$$

By plotting $\ln(K_{eq})$ vs. $1/T$, ΔH° and ΔS° can be obtained from the slope and intercept, respectively.

All equilibrium constants obtained were independent of the partial pressures of the various ethers and the ion source total pressure.

Acetone was obtained from BDH Inc., fluoroacetone from Sigma–Aldrich Canada, 1,1,1-trifluoroacetone from SCM Specialty Chemicals, pentafluoroacetone from Columbia Organic Chemical Co. Inc., hexafluoroacetone from Chemicals Procurement Laboratories Inc., methane from Praxair, and carbon tetrachloride from J.T. Baker Chemical Co. All chemicals were used as received.

2.2. Fourier-transform infrared spectrometry

All IR spectra were recorded on a Bruker IFS-55 FT-IR spectrometer. The fluorinated acetones were introduced in a stainless steel gas cell at room temperature with a path length of 22 cm and at pressures between 5 and 20 Torr. Absorption spectra were recorded from 500 to 5000 cm^{-1} by adding 30 scans at 1 cm^{-1} resolution using AgCl windows.

3. Computational

All computations were performed using the *Gaussian 98* and *Gaussian 98W* suite of programs [16]. Geometries were optimized at the HF [17] and MP2(fc) [18] levels of theory, using the 6-31G(d) basis set (**1**) [19,20] for C, H, O, and F, and the 6-31+G(d) basis set (**3**) [19–23] for Cl. Normal mode vibrational frequencies were calculated at the HF level of theory and scaled by 0.8953 [24], using the same basis sets as those for the HF geometry optimizations. Single point energy calculations were performed at the MP2 level of theory using the 6-311+G(2df,p) basis set (**2**) [21–23,25,26] for C, H, O, and F, and the 6-311++G(3df,3pd) basis set (**4**) [21–23,25,26] for Cl on the MP2 geometries. In addition, for acetone, fluoroacetone, 1,1,1-trifluoroacetone, pentafluoroacetone, hexafluoroacetone, and chloride ion–hexafluoroacetone, geometries were optimized and frequencies determined at the B3LYP level of theory [27–29], using the 6-311++G(3d,3p) basis set (**5**) [21–23,25,26] for C, H, F, and O, and the 6-311++G(3df,3pd) basis set for Cl. For $\text{CF}_3\text{C(O)CF}_3$ and $\text{Cl}^-(\text{CF}_3\text{C(O)CF}_3)$ the HF and B3LYP thermochemistry was also determined using a procedure for treating hindered rotations [30] to correct the entropy, S°_{298}, for hindering of the rotations of the CF_3 groups [31].

Standard ambient deprotonation enthalpy changes, $\Delta_{acid}H^\circ_{298}$, were calculated at the G3 and G3(MP2) levels of theory [11] for a series of small to medium sized organic and inorganic molecules to test the suitability of these composite methods for these systems.

Relaxed potential energy surface scans [30] were performed for $\text{Cl}^-(\text{CH}_3\text{C(O)CH}_3)$ and $\text{Cl}^-(\text{CF}_3\text{C(O)CF}_3)$ at the MP2/[**1**/**3**] level of theory. For some points along the reaction coordinate, the $\text{Cl}^- \cdots \text{CO}$ distance, the structures were optimized to gain additional insight into the complex formation and the factors that determine it. For $\text{Cl}^-(\text{CH}_3\text{C(O)CH}_3)$ this distance was set between 4.0 and 14.0 Å, while for $\text{Cl}^-(\text{CF}_3\text{C(O)CF}_3)$

it was set between 2.2 and 12.2 Å. The step size for both scans was 0.2 Å.

4. Results and discussion

4.1. Structures

In Fig. 1(a)–(h), the structures of acetone and the four fluorinated acetones are shown. In contrast to the study carried out for the chloride ion–fluorinated ether complexes, no other stable rotamers have been sought, except in the case of $CH_3C(O)CH_2F$. Choi and Boyd have previously calculated the structures of the various fluorinated acetones at the HF/STO-3G and 4-31G level of theory [32,33]. The structures of two stable CH_2F group rotamers for this molecule, and one possible enol isomer have been calculated. At the MP2/**1** level of theory the agreement with the experimentally determined structures is good to excellent [34], with the various bond lengths all within 0.015 Å, and the bond angles within 1.3°. Substitution of fluorine for hydrogen atoms has no noticeable effect on the CO and CH bond lengths. The CC bond lengths change relative to acetone, in general with an increase for the methyl group carbon attached to one or more fluorine atoms. In both $CH_3C(O)CH_2F$ and $CF_3C(O)CH_3$, the CH_3–C bond length decreases slightly relative to acetone. Small variations in CF bond lengths are observed, mainly depending upon whether the fluorine atoms are in *syn* or *anti* orientations. There seems to be no clear trend for the effect of fluorine substitution on the CCO bond angle. In general, the relative methyl group orientations are such as to minimize the repulsion among fluorine atoms on remote methyl groups, and between fluorine atoms and the carbonyl oxygen. In the enol isomer of $CH_3C(O)CH_2F$ shown, there is an intramolecular hydrogen bond-like interaction (O–H···F–C) which gives rise to this as the most stable enol isomer. Despite the seemingly favorable structure, the enol isomer is 12.7 kcal mol^{-1} less stable than its keto isomer, calculated at the MP2/**2**//MP2/**1** level of theory. The results for the five (fluorinated) acetones calculated at the B3LYP/**5** level of theory show no real significant deviations in geometry from the MP2/**1** results. For the C=O bond length, the B3LYP/**5** results are in general smaller by 0.017–0.026 Å. For the C–C bond lengths, the MP2/**1** results in general are smaller. For the C–C bond length of CH_3 and CH_2F groups this value is 0.001–0.004 Å, while for the CF_2H and CF_3 groups it is 0.016–0.022 Å. For the C–H and C–F bonds, the B3LYP/**5** results are smaller by 0.002–0.004 and 0.001–0.008 Å, respectively. Finally, the B3LYP/**5** O–C–C bond angles are equal to or smaller than the MP2/**1** results by 0.1–0.7°.

More interesting are the structures of the various chloride ion–acetone complexes that are shown in Fig. 2(a)–(h). Formation of $Cl^-(CH_3C(O)CH_3)$ induces only minor changes in the acetone moiety relative to the uncomplexed acetone. These include small increases in the CO and the *syn* CH bond lengths as well as the CCO bond angle, and a small decrease in the CC and *anti* CH bond lengths. The $Cl^-\cdots H^-C$ bond length of 2.67 Å is of the order of magnitude that would be expected for the ΔH°_{298} value obtained experimentally. This value is 0.15 Å shorter than that found for the same type of bonding found in $Cl^-(CH_3OCH_3)$ [9], which has a much smaller ΔH°_{298} value (−7.3 vs. 13.1 kcal mol^{-1}). For $Cl^-(CH_3C(O)CH_2F)$ two stable rotamers are again possible, which are closely associated with the two neutral rotamers. In Fig. 2(b) the $Cl^-\cdots H^-$–CH_2 and $Cl^-\cdots H^-$–CHF bond lengths are 2.716 and 2.560 Å, respectively, while in Fig. 2(c) they are 2.589 and 2.642 Å, respectively. These are the two most significant differences between these two structures. The $Cl^-(CH_2C(OH)CH_2F)$ complex shows some interesting features compared to its neutral counterpart. Firstly, the chloride ion is interacting with both the O–H group and one of the hydrogen atoms in the CH_2F group. The latter interaction has replaced the intramolecular hydrogen bond, O–H···F–C, in the neutral enol isomer. The $Cl^-\cdots H$–O bond length of 2.088 Å is almost identical to that in $Cl^-(HOCH_3)$ at the MP2(full)/6-311++G(d,p) level of theory [35]. The $Cl^-\cdots H$–CHF bond length of 2.666 Å is much smaller than the $Cl^-\cdots H$–CH_2 bond length of 3.413 Å in $Cl^-(HOCH_3)$. Upon chloride ion complex

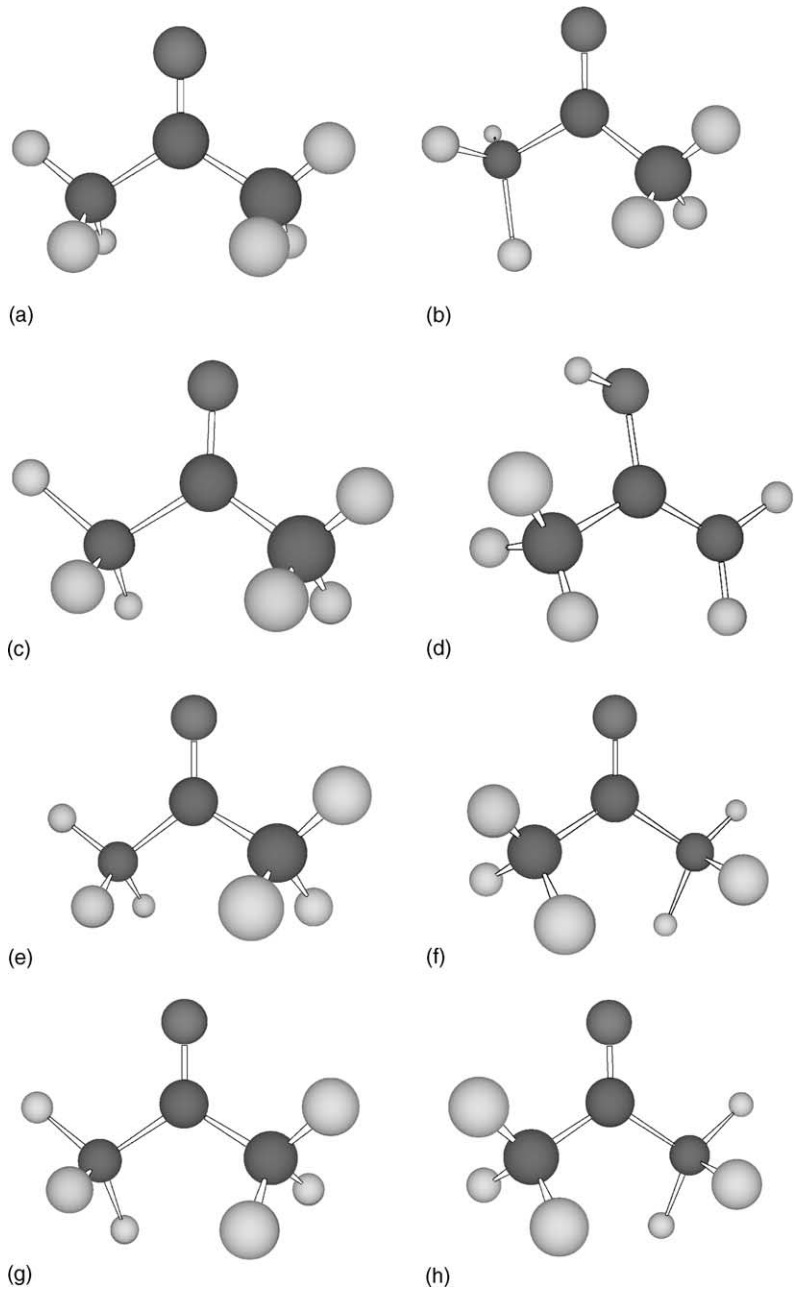

Fig. 1. Optimized MP2(fc)/6-31G(d) geometries of (a) $CH_3C(O)CH_3$, (b) $CH_3C(O)CH_2F$ (rotamer 1), (c) $CH_3C(O)CH_2F$ (rotamer 2), (d) $CH_2C(OH)CH_2F$, (e) $CH_3C(O)CF_3$, (f) $CF_2HC(O)CF_2H$, (g) $CF_3C(O)CF_2H$, and (h) $CF_3C(O)CF_3$.

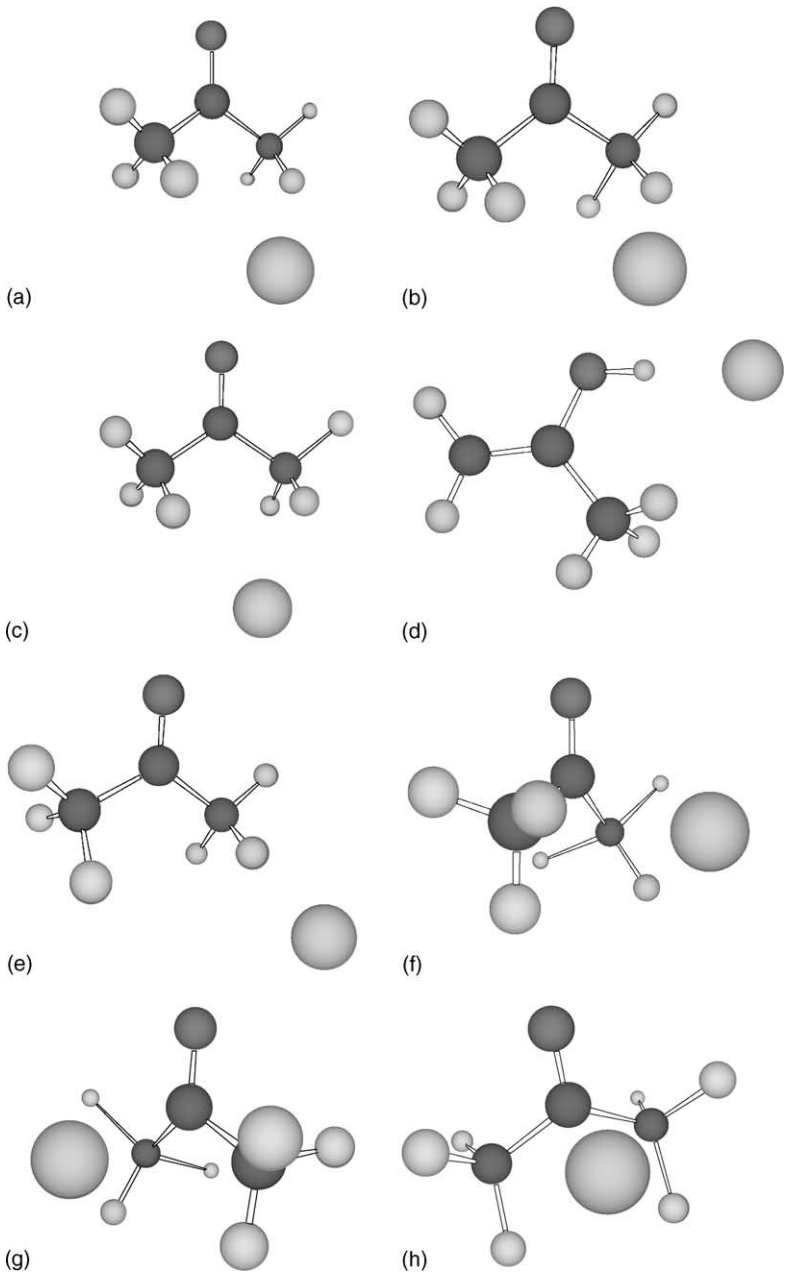

Fig. 2. Optimized MP2(fc)/[6-31+G(d)/6-31G(d)] geometries of (a) $Cl^-(CH_3C(O)CH_3)$, (b) $Cl^-(CH_3C(O)CH_2F)$ (rotamer 1), (c) $Cl^-(CH_3C(O)CH_2F)$ (rotamer 2), (d) $Cl^-(CH_2C(OH)CH_2F)$, (e) $Cl^-(CH_3C(O)CF_3)$, (f) $Cl^-(CF_2HC(O)CF_2H)$, (g) $Cl^-(CF_3C(O)CF_2H)$, and (h) $Cl^-(CF_3C(O)CF_3)$.

formation, the O–H bond length increases from 0.975 to 1.002 Å, while the C–O bond length decreases from 1.372 to 1.355 Å. Finally, the $Cl^- \cdots H$–O bond angle of 173.0° is very close to the $F^- \cdots H$–O bond angle in $F^-(HOCH_3)$ [35].

The structure of the $Cl^-(CH_3C(O)CF_3)$ complex is quite different from the corresponding $Cl^-(CH_3OCF_3)$ complex. In the latter case, the chloride ion interacts with all three methyl group hydrogen atoms, resembling a S_N2 type complex [9]. As shown in Fig. 2(e), the chloride ion interacts only with one of the CH_3 hydrogen atoms. The $Cl^- \cdots H$–CH_2 bond length of 2.375 Å is much smaller than that in $Cl^-(CH_3C(O)CH_3)$, while the $Cl^- \cdots H$–C bond angle is close to being linear. Surprisingly, both the experimental ΔH° and the calculated ΔH°_{298} values are very close. Formation of the chloride complex does not change the structure of the $CF_3C(O)CH_3$ moiety to any significant extent.

The bonding in the $Cl^-(CF_2HC(O)CF_2H)$ complex is fairly similar to that found in $Cl^-(CF_2HOCF_2H)$ [9], although some important differences are present. In the $Cl^-(CF_2HOCF_2H)$ complex, the two $Cl^- \cdots HCF_2$ bond lengths are 2.436 and 2.438 Å, respectively, while in $Cl^-(CF_2HC(O)CF_2H)$ they are 2.700 and 2.726 Å, respectively. These latter two are somewhat larger than those in $Cl^-(CH_3C(O)CH_3)$. At first this seems surprising, since on going from $Cl^-(CH_3OCH_3)$ to $Cl^-(CF_2HOCF_2H)$ there is a large decrease in the $Cl^- \cdots H$–CF_2 bond lengths. In the $Cl^-(CF_2HC(O)CF_2H)$ complex, the $Cl^- \cdots CO$ distance is 2.800 Å, and so it seems that interaction of the chloride ion with the carbonyl group carbon atoms is as important in this case as the hydrogen bonding interactions with the two CF_2H groups. The $Cl^- \cdots H$–CF_2 bond angles in $Cl^-(CF_2HC(O)CF_2H)$ of 97.0 and 102.0°, respectively, are very different from 158.0 and 158.2° in $Cl^-(CF_2HOCF_2H)$.

In the chloride ion–1,1,3,3-tetrafluoro ether complex, the hydrogen bonding is primarily directed along the C–H bond, which may be expected to be more favorable than that in the chloride ion–1,1,3,3-tetrafluoro acetone complex. In the $Cl^-(CF_3C(O)CF_2H)$ complex, the chloride ion seems to prefer interaction with the carbonyl group carbon atom, instead of the very acidic hydrogen atom. The $Cl^- \cdots CO$ distance is 2.524 Å, while the $Cl^- \cdots H$ distance is 2.928 Å. This observation was very surprising, because a priori it had been expected that a complex similar to $Cl^-(CF_3OCF_2H)$ would be obtained. In the $Cl^-(CF_3OCF_2H)$ complex, however, the $Cl^- \cdots H$ distance is 2.282 Å, and the $Cl^- \cdots H$–CF_2 angle is 175.7°. Replacing the ether functional group by a carbonyl group apparently makes a huge difference in bonding characteristics, and it is very interesting to understand what factor(s) is(are) responsible for this. In the chloride ion–hexafluoro acetone complex, $Cl^-(CF_3C(O)CF_3)$, the $Cl^- \cdots CO$ distance is 2.272 Å, much shorter than that in $Cl^-(CF_3C(O)CF_2H)$. Only minor changes in the C=O, C–F, and C–C bond lengths are observed. The O=C–C bond angle decreases from 122.0 to 116.3° upon chloride ion complex formation. The most interesting structural feature in the $Cl^-(CF_3C(O)CF_3)$ complex is the relative orientation of the two CF_3 groups. In the chloride ion complex of hexafluoroacetone, the two CF_3 groups are staggered in such a way as to minimize repulsion between Cl^- and the fluorine atoms. Larson and McMahon speculated on the possibilities of either a tetrahedral-like, covalently bonded complex, $(CF_3)_2ClCO^-$, or an electrostaticly bonded complex where the chloride ion interacts with the carbonyl group carbon atom from below the hexafluoro acetone molecule [10], as shown in Fig. 3. If CN^- is used instead of Cl^-, the formation of a covalently bonded complex, $(CF_3)_2CNCO^-$, is expected to be more likely, especially at relatively low temperatures. In that case, relatively large ΔH° and ΔS° values should be obtained. Computations at the HF/**1** level indicate that $(CF_3)_2CNCO^-$ should exist [36]. At higher temperatures, an electrostaticly bonded complex, $CN^-(CF_3C(O)CF_3)$, may dominate, which

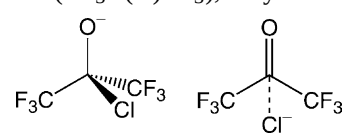

Fig. 3. Proposed covalent and electrostatic chloride ion–hexafluoro acetone complex structures.

should give rise to ΔH° and ΔS° values close to those for $Cl^-(CF_3C(O)CF_3)$. For the B3LYP/[**4**/**5**] structure of $Cl^-(CF_3C(O)CF_3)$ no pronounced changes are observed relative to the MP2/[**1**/**3**] structure. The $Cl^- \cdots CO$ distance is 2.291 Å, and there is a small increase in the C=O bond length from 1.188 Å in $CF_3C(O)CF_3$ to 1.220 Å in $Cl^-(CF_3C(O)CF_3)$.

In Fig. 4(a)–(e), the MP2(full)/**1** structures of the deprotonated acetone, fluoroacetone (two isomers), 1,1,1-trifluoroacetone, and pentafluoroacetone are shown. The structures of the corresponding neutral conjugate acids are essentially identical to the same structures calculated at the MP2(fc)/**1** level of theory. Upon deprotonation, the C–C bond length will decrease, while the C–O bond length will increase. Delocalization of the negative charge gives both the C–C and C–O bonds a formal bond order of 1.5. The O–C–C bond angle for the methyl group from which the proton was abstracted increases to $129 \pm 3^\circ$, while the other O–C–C bond angle decreases to $113 \pm 3^\circ$. No dramatic changes in C–H, C–F, or C–C bond lengths, other than those mentioned above, have been observed.

4.2. Thermochemistry

In Table 1 an overview of the experimental and computational thermochemistry for each of the

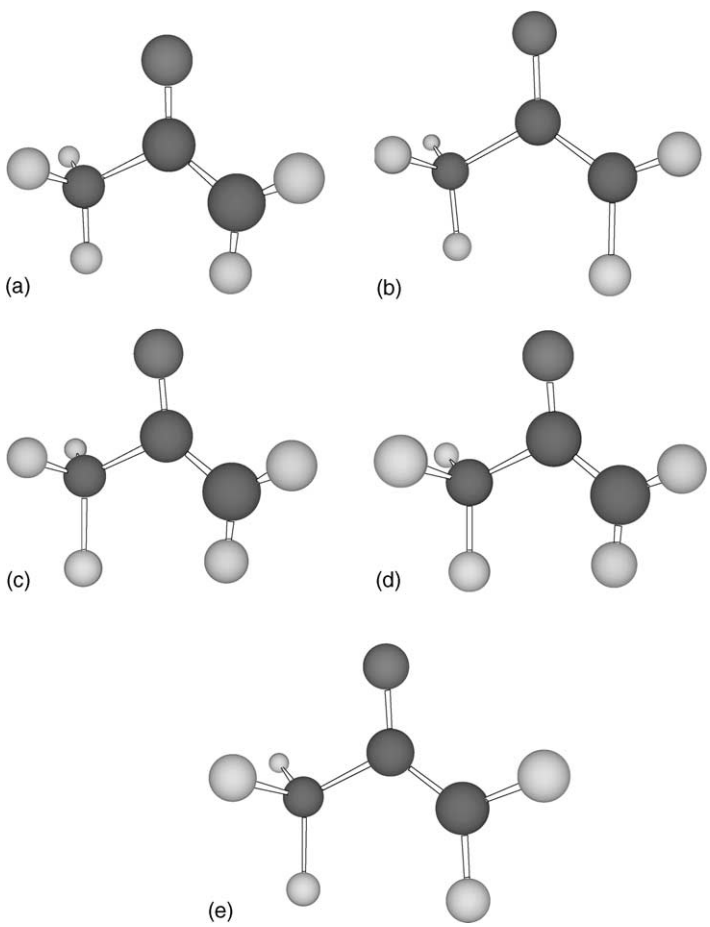

Fig. 4. Optimized MP2(full)/6-31G(d) geometries of (a) $CH_3C(O)CH_2^-$, (b) $CH_3C(O)CHF^-$, (c) $CH_2C(O)CH_2F^-$, (d) $CF_3C(O)CH_2^-$, and (e) $CF_3C(O)CF_2^-$.

Table 1
Experimental and computational enthalpy and entropy changes for chloride ion–fluorinated acetone clustering equilibria

Clustering equilibrium	ΔH° PHPMS (kcal mol^{-1})	ΔH°_{298} MP2//MP2 (kcal mol^{-1})	ΔS° PHPMS (cal mol^{-1} K^{-1})	ΔS°_{298} HF (cal mol^{-1} K^{-1})
$Cl^- + CH_3C(O)CH_3 \rightleftarrows Cl^-(CH_3C(O)CH_3)$	−14.1	−13.1	−20.2	−20.8
$Cl^- + CH_3C(O)CH_2F \rightleftarrows Cl^-(CH_3C(O)CH_2F)$ (rotamer 1)	−18.4	−13.8	−24.5	−20.3
$Cl^- + CH_3C(O)CH_2F \rightleftarrows Cl^-(CH_3C(O)CH_2F)$ (rotamer 2)		−17.8		−22.8
$Cl^- + CH_3C(OH)CHF \rightleftarrows Cl^-(CH_3C(OH)CHF)$		−22.3		−20.7
$Cl^- + CH_3C(O)CF_3 \rightleftarrows Cl^-(CH_3C(O)CF_3)$	−13.7	−13.0	−18.4	−18.7
$Cl^- + CF_2HC(O)CF_2H \rightleftarrows Cl^-(CF_2HC(O)CF_2H)$		−26.4		−21.3
$Cl^- + CF_3C(O)CF_2H \rightleftarrows Cl^-(CF_3C(O)CF_2H)$	−26.1	−26.8	−29.9	−22.2
$Cl^- + CF_3C(O)CF_3 \rightleftarrows Cl^-(CF_3C(O)CF_3)$	−28.8	−27.8	−37.6	−25.2

Estimated relative errors $\Delta H^\circ \pm 0.2$ kcal mol^{-1}, $\Delta S^\circ \pm 1.0$ cal mol^{-1} K^{-1}. Estimated absolute errors $\Delta H^\circ \pm 0.4$ kcal mol^{-1}, $\Delta S^\circ \pm 2.0$ cal mol^{-1} K^{-1}.

chloride ion clustering reactions to fluorinated acetones (Eq. (1)) is shown. In Fig. 5, the experimental Van't Hoff plots are shown from which the clustering ΔH° and ΔS° values were derived. From previous work on chloride ion–ether complexes it had been shown that for the ab initio calculated ΔH°_{298} values, excellent agreement with the experimental ΔH° values could be obtained from high level ab initio calculations at the MP2/[**2**/**4**]//MP2/[**1**/**3**] level of theory [9]. However, there were only a few systems for which good agreement of ΔS°_{298} values, from calculations at the HF/[**1**/**3**] level of theory, with experimental ΔS° values could be obtained. Significant differences in entropy values were obtained for systems where hindering of methyl groups rotations upon chloride ion complex formation occurred. In contrast, as can been seen from Table 1, for the chloride ion–acetone complexes excellent agreement between experiment and theory was obtained for almost all enthalpy changes and most entropy changes as well. For the formation

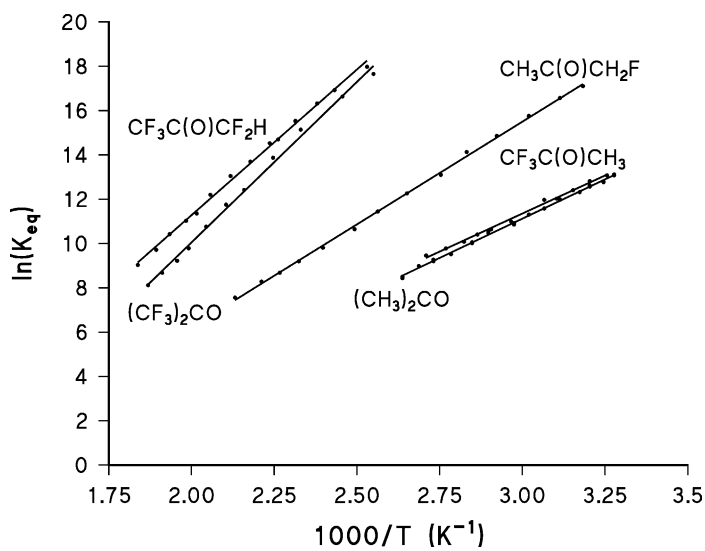

Fig. 5. Van't Hoff plots for chloride ion clustering equilibria with acetone and selected fluoroacetones [$CH_3C(O)CH_3$, $CH_3C(O)CH_2F$, $CF_3C(O)CH_3$, $CF_3C(O)CF_2H$, $CF_3C(O)CF_3$].

of both $Cl^-(CH_3C(O)CH_3)$ and $Cl^-(CH_3C(O)CF_3)$, the agreement for both ΔH° and ΔS° is excellent. This may indicate that in these two complexes, the methyl groups still undergo relatively free rotation. The ΔH° and ΔS° values from the present work for acetone are in excellent agreement with earlier data from this laboratory (-14.2 kcal mol^{-1} and -21.9 cal mol^{-1} K^{-1}, respectively) [37], and data from Kebarle's laboratory (-14.2 kcal mol^{-1} and -21.9 cal mol^{-1} K^{-1}, respectively) [38]. For fluoroacetone two stable rotamers exist (see Fig. 1(b) and (c)) with the first of these 2.2 kcal mol^{-1} more stable. The two rotamers are separated by a barrier of 4.4 kcal mol^{-1}, as calculated at the MP2/**2**//MP2/**1** level of theory. In the $Cl^-(CH_3C(O)CH_2F)$ complex, this has changed to -1.8 and 0.5 kcal mol^{-1}, respectively, as calculated at the MP2/[**2**/**4**]//MP2[**1**/**3**] level of theory. Interestingly, the agreement between experiment and theory for rotamer 2, the higher energy rotamer, is surprising. Unfortunately, no rationalization could be advanced to explain this agreement. No other isomers for $Cl^-(CH_3C(O)CH_2F)$ were found. It was unexpected that the chloride ion should prefer to interact with hydrogens on each of the methyl groups since the $\Delta_{acid}H^\circ_{298}$ value for the CH_3 group is 19.0 kcal mol^{-1} less favorable than that for the CH_2F group, as calculated at the G3(MP2) level of theory (Section 4.3). As already noted above, the gas phase deprotonation enthalpy is not the dominant factor in determining the structure adopted in these systems. For the $Cl^-(CF_3C(O)CF_2H)$ and $Cl^-(CF_3C(O)CF_3)$ complexes, the reason for the large disagreements between the experimental ΔS° and computational ΔS°_{298} values is the same as that advanced for $Cl^-(CF_2HOCF_2H)$. Larson and McMahon measured the ΔG°_{298} values for the formation of $Cl^-(CF_2HC(O)CF_2H)$, $Cl^-(CF_3C(O)CF_2H)$, and $Cl^-(CF_3C(O)CF_3)$ by ICR from exchange equilibria involving chloride ion complexes with known ΔG°_{298} values [10]. Free energy values of -18.1 and -16.3 kcal mol^{-1} for the two latter complexes were obtained [10]. Using the ΔH° and ΔS° values from the present PHPMS study, ΔG°_{298} values for formation of $Cl^-(CF_3C(O)CF_2H)$ and $Cl^-(CF_3C(O)CF_3)$ of (-17.6 ± 1.0) kcal mol^{-1} and (-17.2 ± 1.0) kcal mol^{-1}, respectively were found. By using the ΔG°_{298} value of Larson and McMahon for formation of $Cl^-(CF_3C(O)CF_2H)$, and a ΔH°_{298} of -27.0 kcal mol^{-1} [10], a ΔS°_{298} value of -29.9 cal mol^{-1} K^{-1} can be calculated. This value is somewhat smaller than the PHPMS value -31.3 cal mol^{-1} K^{-1} found for $Cl^-(CF_2HOCF_2H)$ [9], and the difference seems reasonable based on the different structures. The very large ΔS° value for Eq. (6) indicates, as expected from Fig. 2(h), that the two CF_3 group rotations become severely hindered upon complex formation. The large moment of inertia of a CF_3 group will contribute to a more negative ΔS° than, for instance, a CF_2H group, as occurs in $Cl^-(CF_2HOCF_2H)$.

$$Cl^- + CF_3C(O)CF_3 \leftrightarrows Cl^-(CF_3C(O)CF_3) \qquad (6)$$

For the formation of $Cl^-(CF_3C(O)CF_3)$, calculated at the B3LYP/[**4**/**5**] level of theory, ΔH°_{298} and ΔS°_{298} values of -24.9 kcal mol^{-1} and -30.0 cal mol^{-1} K^{-1}, respectively, were found. The fairly large deviation of ΔH°_{298} from ΔH° while using large basis sets associated with the MP2 computations is surprising. On the other hand, the ΔS°_{298} value is closer to the experimental ΔS° value. By using a method developed by Ayala and Schlegel [31], which is implemented in *Gaussian* 98, hindered rotations can be identified [30]. Once a hindered rotation has been identified, automatically modified thermodynamic functions are used to calculate the correct entropy, heat capacity, etc. [31]. Using the B3LYP/[**4**/**5**] level of theory, a S°_{298} value for $Cl^-(CF_3C(O)CF_3)$ of 102.42 cal mol^{-1} K^{-1} was obtained using the harmonic oscillator approximation. Using the hindered rotor approximation a value of 102.70 cal mol^{-1} K^{-1} was determined. At the HF/[**1**/**3**] level of theory values of 106.94 and 111.79 cal mol^{-1} K^{-1} were determined, respectively, indicating that there is a significant dependence on the level of theory used. From the B3LYP/[**4**/**5**] computations one might then conclude that in the $Cl^-(CF_3C(O)CF_3)$ complex, the rotations of the CF_3 groups are not substantially hindered. The difference between the ΔS° value from PHPMS and the ΔS°_{298} value from the B3LYP/[**4**/**5**] computations may then

be due to anharmonic intramolecular vibrations in the $Cl^-(CF_3C(O)CF_3)$ complex.

Since the gas phase deprotonation enthalpy is evidently not the main factor determining the structures of the chloride ion–acetone complexes and the thermochemistry of their formation, then it is important to understand what is the dominant interaction determining structure. The electric dipole moment seems to be a logical first choice. In $Cl^-(CH_3C(O)CH_3)$ the chloride ion is seen not to be aligned along the C=O bond, the direction of the electric dipole moment in acetone. Similar to the situation found for $Cl^-(CH_3OCH_3)$, that particular structure appears to represent a transition state [39]. Identical arguments can be made for the other chloride acetone complexes. In addition to the orientation of the electric dipole moment, its magnitude for the various acetones studied does not seem to correlate with the observed ΔH° values, when assuming ion–dipole interactions. The introduction of fluorine atoms in general increases the polarizability, as can be seen going from CH_4 to CF_4 ($\alpha(CH_4) = 2.59$, $\alpha(CH_3F) = 2.97$, $\alpha(CF_3H) = 3.57$ and $\alpha(CF_4) = 3.84\,Å^3$) [34]. This increase works out to be approximately $0.31\,Å^3$ per fluorine atom. It seems reasonable that this kind of behavior applies to the fluorinated acetones as well, relative to acetone itself. The change in going from ethane to hexafluoroethane is an increase in polarizability from 4.47 to $6.82\,Å^3$ [34]. This corresponds to an increase of $0.39\,Å^3$ per fluorine atom. From ethane to acetone the polarizability increases to $6.39\,Å^3$ [34]. These trends then indicate that the ion-induced dipole moment may be mainly responsible for the magnitude of the observed trends in thermochemistry. Unfortunately, no reliable values for the polarizabilities from the HF/**1** computations may be expected, and computations at, for instance, the QCISD(fc)/6-311++G(3df,2pd) [40] level of theory are not feasible for these systems. The influence of ion–quadrupole interaction, especially in $CF_3C(O)CF_3$, may not be excluded, but the exact orientation of the quadrupole moment of $CF_3C(O)CF_3$ has not been determined to the best of our knowledge. The importance of ion–quadrupole interactions in negative gas phase cluster ions has been recently noted for $Na^+(C_6H_6)$ [41] and $Cl^-(C_6F_6)$ [36] complexes where the chloride ion seems to interact with the π cloud above the ring, which is the *z*-axis direction of the quadrupole moment of both C_6F_6 and C_6H_6.

4.3. Gas phase acidities of fluorinated acetones

Farid and McMahon have previously determined approximate standard ambient gas phase deprotonation enthalpies for acetone and five fluorinated acetones by bracketing experiments using ICR experiments (Eq. (7)) [42].

$$C_3F_nH_{6-n}O + B^- \leftrightarrows C_3F_nH_{5-n}O^- + BH \quad (7)$$

The results indicated that fluorine substitution provides a net stabilizing effect on planar carbanions, although the increase in stability can be considered to be irregular [42]. Initially it was assumed that there might be a direct correlation between the enthalpy change for the various reactions of Eq. (1), ΔH°, and the deprotonation enthalpy (Eq. (8)), $\Delta_{acid}H^\circ$.

$$C_3H_nF_{6-n}O \rightarrow C_3H_{n-1}F_{6-n}O^- + H^+ \quad (8)$$

$\Delta_{acid}H^\circ_{298}$ values for acetone and the four fluorinated acetones used were calculated at the G3(MP2) level of theory. In order to verify the suitability of G3(MP2) to calculate accurate $\Delta_{acid}H^\circ_{298}$ values, test calculations on a series of small to medium sized organic and inorganic acids were performed at the G3 and G3(MP2) level of theory and compared to literature data [43].

In Table 2, the calculated H°_{298} values from the G3 and G3(MP2) calculations are shown for the various acids and their conjugated bases. These H°_{298} values were converted to $\Delta_{acid}H^\circ_{298}$ values for the HA $\rightarrow$ $H^+ + A^-$ reactions using Eq. (9).

$$\Delta_{acid}H^\circ_{298}(HA) = H^\circ_{298}(H^+) + H^\circ_{298}(A^-) - H^\circ_{298}(HA) \quad (9)$$

In Eq. (9), H°_{298} (H^+) is taken as 0.002360 hartree. As can be seen from Table 3, there is very close agreement between the G3 and G3(MP2) results, and in most cases, between the computational and experimental data. DeTuri et al. showed, for H_2O,

Table 2
G3(MP2) and G3 standard ambient enthalpies of relevant species

Neutral	H°_{298}(G3(MP2)) (hartree)	H°_{298}(G3) (hartree)	Anion	H°_{298}(G3(MP2)) (hartree)	H°_{298}(G3) (hartree)
HF	−100.355477	−100.397801	F^-	−99.763933	−99.806828
HCl	−460.349212	−460.651359	Cl^-	−459.819999	−460.121239
H_2O	−76.338628	−76.378265	HO^-	−75.717174	−75.756934
CH_3OH	−115.547922	−115.624915	CH_3O^-	−114.939055	−115.015963
CF_3OH	−413.076586		CF_3O^-	−412.554319	
C_2H_2	−77.198153	−77.272275	C_2H^-	−76.598215	−76.671128
CH_3CO_2H	−228.777174	−228.934396	$CH_3CO_2^-$	−228.224276	−228.382205
CF_3CO_2H	−526.263532		$CF_3CO_2^-$	−525.748266	
$CH_3C(O)CH_3$	−192.838667	−192.990774	$CH_3C(O)CH_2^-$	−192.252102	−192.403867
$CH_3C(O)CH_2F$	−291.991094		$CH_3C(O)CHF^-$	−291.408062	
			$CH_2C(O)CH_2F^-$	−291.417117	
$CF_3C(O)CH_3$	−490.333258		$CF_3C(O)CH_2^-$	−489.778498	
$CF_3C(O)CF_2H$	−688.640700		$CF_3C(O)CF_2^-$	−688.089959	

CH_3OH, C_2H_2, and HF, that MP2, in combination with the 6-311+G(d,p) and 6-311++G(d,p) basis sets, G2, and G2(MP2) gave mean absolute deviations from experimental data of 0.5, 0.5, 0.7, and 0.7 kcal mol^{-1}, respectively [44]. For the $\Delta_{acid}H^{\circ}_{298}$ values of $CH_3C(O)CH_2F$ (2), and $CF_3C(O)CF_2H$ there seem to be some larger discrepancies from the ICR data from Farid and McMahon; however for $CF_3C(O)CH_3$ there is superb agreement [42]. The difficulty associated with G3 calculations involving molecules with fluorine substitution on sp^2 carbons has been noted previously by Bacskay and co-workers [51]. As discussed above, there appears to be a hydrogen bonding interaction in the chloride ion–acetone complexes investigated, but it seems less pronounced than might have been anticipated. Most notably, the data for $Cl^-(CF_3C(O)CF_2H)$ complex, with its highly acidic hydrogen atom, seems to be in conflict with the ICR results of Farid and McMahon. Under low pressure ICR conditions, the equilibrium shown in

Table 3
G3(MP2), G3, and experimental standard ambient deprotonation enthalpies

Neutral	$\Delta_{acid}H^{\circ}_{298}$(G3(MP2)) (kcal mol^{-1})	$\Delta_{acid}H^{\circ}_{298}$(G3) (kcal mol^{-1})	$\Delta_{acid}H^{\circ}_{298}$ (exp) (kcal mol^{-1})
HF	372.7	372.3	371.6
HCl	333.6	334.1	333.4
H_2O	391.4	391.4	390.7
CH_3OH	383.6	383.6	381.8
CF_3OH	329.2		329.8
C_2H_2	377.9	378.7	378.0
CH_3CO_2H	348.4	348.0	348.1
CF_3CO_2H	324.8		323.8
$CH_3C(O)CH_2$–H	369.6	369.8	369.1
$CH_3C(O)CHF$–H	367.3		366.1[a]
H–$CH_2C(O)CH_2F$	361.7		357.1[a]
$CF_3C(O)CH_2$–H	349.6		349.5
$CF_3C(O)CF_2$–H	347.1		337.6

[a] The order of gas phase acidities of these two compounds has been reversed relative to that given in [42] based on the ab initio calculations reported here which suggest that the carbanion with remote fluorine substitution is the more stable.

Eq. (10) was observed [42].

$$CF_3C(O)CF_2^- + HCl \leftrightarrows CF_3C(O)CF_2H + Cl^- \quad (10)$$

Proton transfer from the $Cl^-(CF_3C(O)CF_2H)$ complex, as shown in Fig. 2(g), would seem not to be a favorable process. In addition, the difference in the G3(MP2) $\Delta_{acid}H^\circ_{298}$ values between $CF_3C(O)CF_2H$ and HCl would prevent an exothermic proton transfer. The only explanation to rationalize the observed proton transfer is the possibility that the endothermic proton transfer reaction may have been entropy driven. Finally, it seems surprising that in the $Cl^-(CH_3C(O)CH_2F)$ complex chloride ion prefers to interact with two hydrogens on separate methyl groups, even though the G3(MP2) $\Delta_{acid}H^\circ_{298}$ value of the CH_2–H group is 19.0 kcal mol^{-1} less favorable than the CHF–H group. Attempts to locate other stable minima where chloride ion interacts exclusively with the CH_3 group, either by single or multiple hydrogen bonding, failed.

4.4. Normal mode vibrational frequencies and intensities

In Tables 4–8, the scaled (0.8953) HF/**1** and unscaled B3LYP/**5** normal mode vibrational frequencies plus IR intensities are tabulated for $CH_3C(O)CH_3$, $CH_3C(O)CH_2F$, $CF_3C(O)CH_3$, $CF_3C(O)CF_2H$, and $CF_3C(O)CF_3$. Simulated IR spectra were also constructed according to the method of Good and Francisco [45] and in general there is very good agreement between experiment and theory, both in general appearance of the spectra and for the different individual frequencies. The FT-IR spectra obtained for $CF_3C(O)CH_3$ and $CF_3C(O)CF_3$ show excellent

Table 4
Calculated, scaled HF/6-31G(d) and B3LYP/6-311++G(3d,3p), and experimental normal mode vibrational frequencies, and infrared intensities of acetone

Mode	HF/6-31G(d)		B3LYP/6-311++G(3d,3p)		Experiment	
	ν (cm^{-1})	Int$_{abs}$ (km mol^{-1})	ν (cm^{-1})	Int$_{abs}$ (km mol^{-1})	ν (cm^{-1})	Int$_{rel}$
1	45	0	35	0	105	
2	128	0	133	0	109	
3	359	1	379	2	385	W
4	476	3	490	1	484	W
5	515	23	534	14	530	M
6	758	0	782	2	777	W
7	878	0	885	0	877	
8	880	4	886	9	891	M
9	1066	1	1083	0	1066	
10	1110	3	1118	3	1091	M
11	1210	76	1233	71	1216	S
12	1384	8	1388	18	1364	S
13	1392	49	1389	55	1364	S
14	1439	0	1464	0	1410	M
15	1442	0	1468	2	1426	
16	1445	21	1474	30	1435	M
17	1461	18	1492	19	1454	M
18	1810	229	1783	197	1731	S
19	2868	4	3021	1	2937	M
20	2875	12	3028	7	2937	M
21	2917	0	3074	0	2963	
22	2925	39	3081	17	2972	M
23	2975	15	3135	12	3019	M
24	2976	14	3136	6	3019	M

HF/6-31G(d) frequencies scaled by 0.8953.

Table 5
Calculated, scaled HF/6-31G(d) and B3LYP/6-311++G(3d,3p), and experimental normal mode vibrational frequencies, and infrared intensities of fluoroacetone (values for rotamer 2 in parentheses)

Mode	HF/6-31G(d)		B3LYP/6-311++G(3d,3p)		Experiment	
	ν (cm^{-1})	Int_{abs} (km mol^{-1})	ν (cm^{-1})	Int_{abs} (km mol^{-1})	ν (cm^{-1})	Int_{rel}
1	60 (17)	17 (2)	69 (51)	16 (1)		
2	149 (105)	0 (2)	128 (111)	0 (2)		
3	240 (245)	14 (1)	239 (248)	13 (1)		
4	459 (379)	5 (1)	471 (392)	1 (1)		
5	477 (451)	33 (4)	491 (464)	16 (1)		
6	493 (589)	4 (37)	502 (606)	12 (24)		
7	749 (800)	2 (7)	771 (808)	4 (1)	776	W
8	860 (861)	2 (3)	861 (857)	1 (3)	858	W
9	984 (937)	1 (34)	991 (954)	5 (43)		
10	1081 (1093)	107 (0)	1046 (1094)	106 (7)	1059	S
11	1092 (1113)	0 (127)	1095 (1097)	1 (104)	1070	S
12	1229 (1181)	60 (27)	1247 (1194)	57 (27)	1230	M
13	1232 (1249)	3 (0)	1253 (1272)	2 (0)		
14	1375 (1386)	27 (27)	1372 (1387)	10 (28)	1362	M
15	1390 (1419)	28 (9)	1392 (1402)	35 (10)	1373	M
16	1438 (1443)	20 (6)	1460 (1464)	15 (2)		
17	1447 (1451)	9 (11)	1466 (1471)	20 (21)	1436	M
18	1465 (1472)	6 (4)	1469 (1481)	10 (9)		
19	1814 (1832)	207 (212)	1788 (1812)	173 (180)	1751	S
20	2884 (2871)	3 (2)	3033 (3015)	0 (17)		
21	2921 (2893)	17 (27)	3049 (3028)	12 (8)	2873	W
22	2939 (2920)	10 (2)	3085 (3056)	3 (10)	2943	W
23	2970 (2932)	21 (48)	3100 (3082)	6 (10)	2960	W
24	2982 (2980)	12 (9)	3144 (3137)	6 (4)	2978	W

HF/6-31G(d) frequencies scaled by 0.8953.

agreement with spectra from the NIST database [12]. For both the HF/**1** and B3LYP/**5** results, the frequencies below 1100 cm^{-1} show good to excellent agreement, while above 1100 cm^{-1} larger deviations from experimental data become more common. The B3LYP/**5** computations were performed to obtain more accurate IR absorption intensities. Unfortunately, few experimental values are known. For CF_4, C_2F_6, and some fluorinated ethers data have been obtained experimentally. de Oliveira et al. obtained excellent agreement with experiments for CF_nH_{4-n} (n = 0–4) using the B3LYP/**5** level of theory [46]. Applying this same level of theory to C_2F_6 also gave good agreement with recent experimental data from Ballard et al. [47] who found values of 714 cm^{-1} ((37.9 ± 1.2) km mol^{-1}), 1116 cm^{-1} ((284.8 ± 4.2) km mol^{-1}), and 1250 cm^{-1} ((1020.1 ± 18.1) km mol^{-1}), while the B3LYP/**5** computation gave values of 703 cm^{-1} (32 km mol^{-1}), 1099 cm^{-1} (285 km mol^{-1}), and 1250 cm^{-1} (1096 km mol^{-1}). Calculations at the MP2/6-31G(d,p) level of theory by Papasavva et al., showed very good agreement with experimental IR intensities [48], but the normal mode vibrational frequencies deviate more than the B3LYP/**5** results. Recently, Good and Francisco obtained the FT-IR spectra of CH_3OCF_3, $(CF_2H)_2O$, and CF_3OCF_2H and calculated the normal mode vibrational frequencies at various levels of theory [45]. The best agreement (rms error of 2.7%) between experiment and theory was obtained using the B3LYP/**4** level of theory, and these results were used to assign the various modes. The HF/**1** results scaled by 0.8953 from this work in general agree very well [9]. Surprisingly, no experimental FT-IR spectra of $CH_3C(O)CH_2F$ and $CF_3C(O)CF_2H$ are available in the NIST/EPA Gas-Phase Infrared Database [12]. There are FT-IR spectra available for

Table 6
Calculated, scaled HF/6-31G(d) and B3LYP/6-311++G(3d,3p), and experimental normal mode vibrational frequencies, and infrared intensities of 1,1,1-trifluoroacetone

Mode	HF/6-31G(d)		B3LYP/6-311++G(3d,3p)		Experiment	
	ν (cm^{-1})	Int_{abs} (km mol^{-1})	ν (cm^{-1})	Int_{abs} (km mol^{-1})	ν (cm^{-1})	Int_{rel}
1	28	5	32	5		
2	107	1	114	0		
3	223	6	227	5		
4	230	3	231	2		
5	353	1	358	1		
6	416	4	414	2		
7	486	7	492	2		
8	550	18	551	10	564	W
9	600	35	616	28	616	W
10	620	1	622	1		
11	755	2	754	1		
12	955	26	966	34	965	W
13	1038	20	1035	67	1024	W
14	1110	174	1116	147	1115	S
15	1211	293	1119	209	1163	S
16	1270	287	1194	245	1227	S
17	1352	85	1311	35	1331	W
18	1399	2	1396	21		
19	1444	23	1470	25	1432	W
20	1446	10	1472	10		
21	1855	162	1833	152	1782	M
22	2888	1	3040	0	2871	W
23	2946	5	3096	1	2976	W
24	2988	6	3149	3	3029	W

HF/6-31G(d) frequencies scaled by 0.8953.

$CH_3C(O)CH_3$, $CH_3C(O)CF_3$, and $CF_3C(O)CF_3$. The proximity of the calculated normal mode vibrational frequencies relative to experimental results is not very important for calculating thermochemical data for modes at relatively high frequency. Such agreement may become more important for instance when doing Master Equation modeling to interpret the kinetics of ZTRID experiments or RRKM modeling for calculating unimolecular dissociation constants [49]. In those cases both the frequency and the IR intensities need to be known. No attempts were made to assign the various normal mode vibrational frequencies as was done by Good and Francisco. It should be noted also that no detailed discussion will be provided here on the differences between the two methods relative to each other and relative to the experimental data. Only general trends will be discussed. Going from $CH_3C(O)CH_3$ to $CF_3C(O)CF_3$ the frequency of the CO stretch increases by approximately 80 cm^{-1}, and both the HF/**1** and B3LYP/**5** results follow that same trend, even though the absolute values may be off by as much as 80 cm^{-1}. More important is the fact that the relative intensity of the CO stretch decreases in favor of C–C and C–F stretches in the 800–1500 cm^{-1} range. This makes chloride ion complexes of these fluorinated acetones and some ethers ideal model systems for ZTRID experiments in a FT-IR instrument. The strong blackbody IR absorption in this region will most likely promote fast dissociation kinetics of even relatively strongly bound complexes. The introduction of more fluorine atoms also causes the absolute IR intensities of the CO stretch of the HF/**1** and B3LYP/**5** results to be in better accord.

The general appearances of the simulated HF/**1** and B3LYP/**5** IR spectra relative to the FT-IR spectra show no clear trends, and a similar statement can be made

Table 7
Calculated, scaled HF/6-31G(d) and B3LYP/6-311++G(3d,3p), and experimental normal mode vibrational frequencies, and infrared intensities of pentafluoroacetone

Mode	HF/6-31G(d)		B3LYP/6-311++G(3d,3p)		Experiment	
	ν (cm^{-1})	Int_{abs} ($km\,mol^{-1}$)	ν (cm^{-1})	Int_{abs} ($km\,mol^{-1}$)	ν (cm^{-1})	Int_{rel}
1	41	1	41	1		
2	55	1	47	1		
3	149	1	150	0		
4	205	12	206	8		
5	276	8	274	5		
6	310	2	311	2		
7	353	2	345	2		
8	434	17	428	9		
9	490	16	497	8		
10	536	3	541	4		
11	577	2	576	3		
12	633	42	651	31	727	W
13	739	22	740	14	865	W
14	867	76	866	55	895	W
15	1027	150	1002	139	1024	W
16	1143	113	1083	95	1107	W
17	1180	47	1134	175	1163	W
18	1233	348	1163	166	1193	S
19	1272	305	1195	288	1238	M
20	1334	71	1282	76	1311	W
21	1379	95	1356	21	1352	W
22	1417	77	1389	23		
23	1885	100	1866	95	1801	W
24	2978	25	3068	13	2994	W

HF/6-31G(d) frequencies scaled by 0.8953.

for the individual peaks and their calculated absolute IR intensities. HF/**1** computations are less CPU intensive than the B3LYP/**5** computations, but the quality of the results is of higher priority. As long as there are no experimental absolute IR intensities for these compounds available, a thorough test of the two methods is impossible.

More interesting is the effect of chloride ion complex formation upon the IR spectrum of the neutral. In Fig. 6 the simulated IR spectra of $CF_3C(O)CF_3$ at the B3LYP/**5** level of theory and $Cl^-(CF_3C(O)CF_3)$ at the B3LYP/[**4**/**5**] level of theory are shown. The most obvious change is the large shift in the CO stretch frequency of $-215\,cm^{-1}$, and a large increase in the absolute IR intensity of $+239\,km\,mol^{-1}$. Most other peaks in the 600–1400 cm^{-1} range show shifts to smaller wave numbers, while both increases and decreases in the absolute IR intensities take place. These features would make the $Cl^-(CF_3C(O)CF_3)$ an interesting system on which to perform ZTRID experiments (Eq. (11)).

$$Cl^-(CF_3C(O)CF_3) + nh\nu \rightarrow Cl^- + CF_3C(O)CF_3 \quad (11)$$

Obtaining the unimolecular dissociation constants, $k_{uni}(T)$, at different absolute temperatures and performing Master Equation modeling using the DFT data for input of the normal mode vibrational frequencies and corresponding absolute IR intensities would also provide a good test for the quality of the computations. Upon complex formation with chloride ion three new, intramolecular normal mode vibrations are introduced, and both red and blue shifts are observed for the other vibrations already present in the neutral molecules. There is no clear correlation between the

Table 8
Calculated, scaled HF/6-31G(d) and B3LYP/6-311++G(3d,3p), and experimental normal mode vibrational frequencies, and infrared intensities of hexafluoroacetone

Mode	HF/6-31G(d)		B3LYP/6-311++G(3d,3p)		Experiment	
	ν (cm^{-1})	Int_{abs} (km mol^{-1})	ν (cm^{-1})	Int_{abs} (km mol^{-1})	ν (cm^{-1})	Int_{rel}
1	42	0	39	0		
2	45	0	43	0		
3	143	1	145	1		
4	189	11	191	6		
5	258	0	255	0		
6	274	7	271	5		
7	313	1	311	0		
8	365	1	366	0		
9	463	10	462	6		
10	491	13	496	6		
11	518	14	521	9		
12	524	0	530	0		
13	622	1	623	4		
14	702	77	709	53	717	W
15	763	2	761	0		
16	790	12	783	17	779	W
17	968	245	960	214	974	M
18	1213	2	1115	1		
19	1242	70	1160	58	1073	W
20	1265	239	1177	509	1219	S
21	1269	581	1224	333	1259	M
22	1317	335	1242	110	1274	M
23	1377	217	1310	151	1342	M
24	1895	83	1875	85	1807	W

HF/6-31G(d) frequencies scaled by 0.8953.

shift in C–H normal mode vibrations, $\Delta\nu$(C–H), and ΔH°_{298}, as was observed for $\Delta\nu$(RO–H) in X^-(HOR) clusters (X = F, Cl, Br, I; R = CH_3, CH_3CH_2, $(CH_3)_2CH$, $(CH_3)_3C$) [35].

VPDS experiments would clearly be an excellent means to investigate the C–H stretches in the different Cl^-(ether) and Cl^-(acetone) complexes [50].

4.5. Potential energy surfaces

In Figs. 7 and 8, the MP2(fc)/[**1**/**3**] partial potential energy surfaces are shown for the approach of Cl^- along the CO bond dipole axis leading to formation of the $Cl^-(CH_3C(O)CH_3)$ and $Cl^-(CF_3C(O)CF_3)$ complexes. For the reaction coordinate, the $Cl^- \cdots CO$ distance is chosen. It should be noted that at the level of theory used, no reliable energetics can be determined, but a qualitative view of this mode of approach may be obtained.

It has been shown above that chloride ion binds much more strongly to hexafluoro acetone than to acetone itself. From Figs. 7 and 8 it can be seen that the well for $Cl^-(CF_3C(O)CF_3)$ becomes much steeper at relatively short distances and then plateaus at an equilibrium $Cl^- \cdots CO$ distance of ~6 Å. The well for the $Cl^-(CH_3C(O)CH_3)$ complex is less steep and plateaus at an equilibrium $Cl^- \cdots CO$ distance of 8–10 Å. Inspection of structures along the two reaction coordinates clearly indicates that the chloride ion approaches $CH_3C(O)CH_3$ and $CF_3C(O)CF_3$ very differently. At distances longer than 8.0 Å chloride ion interacts with acetone with an alignment along the C=O bond axis, which is also the direction of the dipole moment of acetone. As the chloride ion gets

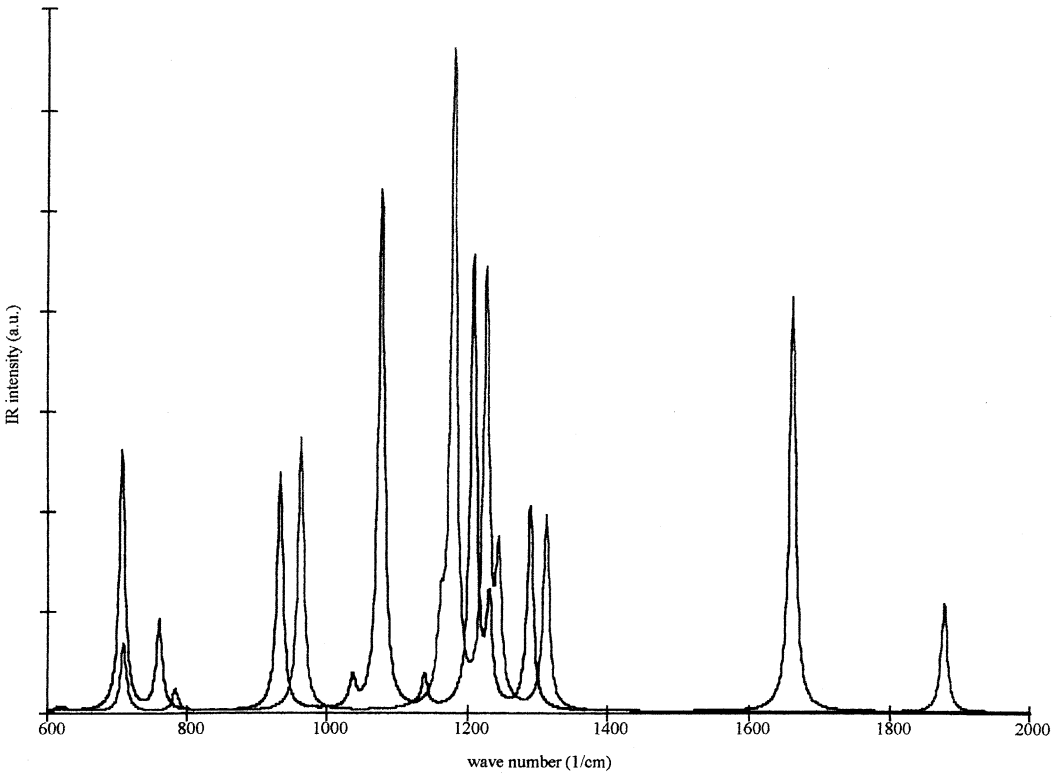

Fig. 6. Simulated IR spectra overlaid of (a) $CF_3C(O)CF_3$ at the B3LYP/**5** level of theory, and (b) $Cl^-(CF_3C(O)CF_3)$ at the B3LYP/[**4**/**5**] level of theory see text for details.

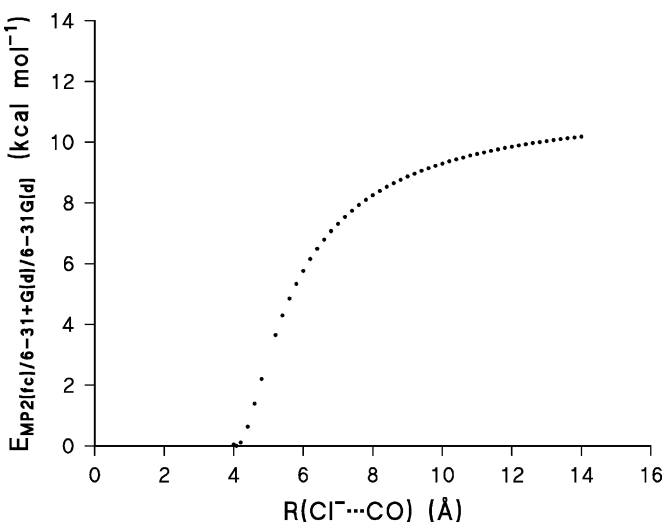

Fig. 7. Relaxed scan 2D potential energy profile at the MP2(fc)/[6-31+G(d)/6-31G(d)] level of theory for the dissociation of the $Cl^-(CH_3C(O)CH_3)$ complex.

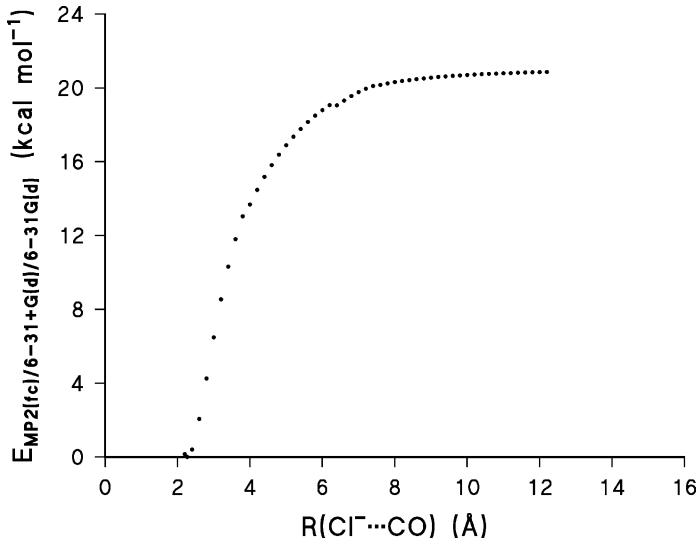

Fig. 8. Relaxed scan 2D potential energy profile at the MP2(fc)/[6-31+G(d)/6-31G(d)] level of theory for the dissociation of the $Cl^-(CF_3C(O)CF_3)$ complex.

closer it deviates from this original approach and begins to interact more with the two hydrogen atoms as found in the equilibrium structure. For hexafluoroacetone a completely different picture emerges. Even though the dipole moment of $CF_3C(O)CF_3$ is still aligned along the C=O bond, the chloride ion does not approach along this alignment because of repulsion with the electronegative fluorine atoms. Instead it will approaches side on, from a general direction which is perpendicular to the plane of the three carbons and the oxygen atoms. As the chloride ion gets closer to the C=O carbon atom, the CF_3 groups begin to rotate away to minimize the repulsion between chloride ion and the fluorine atoms. This process starts taking place at a $Cl^- \cdots CO$ distance of ∼4.0 Å. These two examples then nicely illustrate that the whole process of complex formation can be quite complicated. By simply looking at the equilibrium structure of an ion–molecule complex, it is not possible to tell by what path the ion and neutral molecule approached each other. The reverse trajectory will be followed when the two chloride ion complexes dissociate under the influence of collisions or light.

5. Conclusion

The ΔH° and ΔS° values obtained by PHPMS for chloride ion clustering onto several fluorinated acetones indicate a strong influence of the fluorine substitution pattern on the thermochemistry of adducts formation. The experimental results are supported by high level ab initio calculations at the MP2/[6-311++G(3df,3pd)/6-311+G(2df,p)]//MP2/[6-31+G(d)/6-31G(d)] level of theory. The structures of the various chloride ion–acetone complexes, obtained at the MP2/[6-31+G(d)/6-31G(d)] level of theory, show some unexpected bonding characteristics. In the $Cl^-(CF_3C(O)CF_2H)$ complex, chloride ion does not interact with the highly acidic hydrogen atom. Upon complexation with chloride ion, both CF_3 group rotations in $CF_3C(O)CF_3$ become hindered, thus giving rise to a large negative ΔS° value of $-37.6\,\text{cal mol}^{-1}\,\text{K}^{-1}$. Unfortunately, this value could not be reproduced from the HF and B3LYP computations, even when the entropies were corrected for the occurrence of hindered rotations of the CF_3 groups. The standard ambient deprotonation enthalpy changes, $\Delta_{\text{acid}}H^\circ_{298}$, have been calculated for a series

of small to medium sized organic and inorganic acids using the G3 and G3(MP2) composite methods, and using G3(MP2) for the (fluorinated) acetones. In general, good to excellent agreement with experimental data was obtained. For the fluorinated acetones, some discrepancies with experimental data from Farid and McMahon, obtained by ICR, were observed. No direct correlation between ΔH° and $\Delta_{acid}H^\circ$ seems to exist. Instead, it seems that the observed trends are mainly the result of ion-induced dipole interactions and, to a lesser extent, by ion–dipole interaction. This latter statement is based on the fact that chloride ion does not align with the molecular dipole moment in the various chloride ion–fluorinated acetone adducts. Finally, normal mode vibrational frequencies of $CF_3C(O)CH_3$ and $CF_3C(O)CF_2H$ calculated at the HF/6-31G(d) level of theory, and scaled by 0.8953, seem to agree well with experimental data.

Acknowledgements

The authors gratefully acknowledge the Natural Sciences and Engineering Research Council of Canada (NSERC) for continuing financial support. Steven Lee is acknowledged for assistance with some of the PHPMS experiments and Dustin Dickens for recording the FT-IR spectra.

References

[1] S.M. Blair, J.S. Brodbelt, A.P. Marchand, K.A. Kumar, H.-S. Chong, Anal. Chem. 72 (2000) 2433 and references cited therein.
[2] M. More, D. Ray, P.D. Armentrout, J. Am. Chem. Soc. 121 (1999) 417 and references cited therein.
[3] S.E. Barlow, M.D. Tinkle, Rapid Commun. Mass Spectrom. 13 (1999) 390 and references cited therein.
[4] A. Mele, D. Pezzetta, A. Selvaa, Int. J. Mass Spectrom. 193 (1999) L1.
[5] K.B. Reiche, I. Starke, E. Kleinpeter, H.-J. Holdt, Rapid Commun. Mass Spectrom. 12 (1998) 1021 and references cited therein.
[6] D.V. Dearden, I.-H. Chu, J. Inclsn. Phenom. Mol. Recog. Chem. 29 (1997) 269 and references cited therein.
[7] F.P. Schmidtchen, M. Berger, Chem. Rev. 97 (1997) 1609 and references cited therein.
[8] J. Scheerder, J.F.J. Engbersen, D. Reinhoudt, N. Recl. Trav. Chim. Pays-Bas 115 (1996) 307 and references cited therein.
[9] B. Bogdanov, H.J.S. Lee, T.B. McMahon, Int. J. Mass Spectrom., submitted for publication.
[10] J.W. Larson, T.B. McMahon, J. Phys. Chem. 88 (1984) 1083.
[11] L.A. Curtiss, K. Raghavachari, P.C. Redfern, V. Rasolov, J.A. Pople, J. Chem. Phys. 109 (1998) 7764.
[12] http://webbook.nist.gov/chemistry/
[13] J.E. Szulejko, J.J. Fisher, T.B. McMahon, J. Wronka, Int. J. Mass Spectrom. Ion Process. 83 (1988) 147.
[14] P. Kebarle, Pulsed high pressure mass spectrometry, in: J.M. Farrer, W.H. Saunders Jr. (Eds.), Techniques for the Study of Ion–Molecule Reactions, Wiley/Interscience, New York, NY, 1988, p. 221 and references cited therein.
[15] M. Meot-Ner (Mautner), L.W. Sieck, Int. J. Mass Spectrom. Ion Process. 109 (1991) 187 and references cited therein.
[16] M.J. Frisch, G.W. Trucks, H.B. Schlegel, G.E. Scuseria, M.A. Robb, J.R. Cheeseman, V.G. Zakrzewski, J.A. Montgomery Jr., R.E. Stratmann, J.C. Burant, S. Dapprich, J.M. Millam, A.D. Daniels, K.N. Kudin, M.C. Strain, O. Farkas, J. Tomasi, V. Barone, M. Cossi, R. Cammi, B. Mennucci, C. Pomelli, C. Adamo, S. Clifford, J. Ochterski, G.A. Petersson, P.Y. Ayala, Q. Cui, K. Morokuma, D.K. Malick, A.D. Rabuck, K. Raghavachari, J.B. Foresman, J. Cioslowski, J.V. Ortiz, A.G. Baboul, B.B. Stefanov, G. Liu, A. Liashenko, P. Piskorz, I. Komaromi, R. Gomperts, R.L. Martin, D.J. Fox, T. Keith, M.A. Al-Laham, C.Y. Peng, A. Nanayakkara, C. Gonzalez, M. Challacombe, M.W. Gill, B. Johnson, W. Chen, M.W. Wong, J.L. Andres, C. Gonzalez, M. Head-Gordon, E.S. Replogle, J.A. Pople, Gaussian 98, Revision A.7 Gaussian, Inc., Pittsburgh PA, 1998.
[17] C.C.J. Roothaan, Rev. Mod. Phys. 23 (1951) 69.
[18] C. Møller, M.S. Plesset, Phys. Rev. 46 (1934) 618.
[19] P.C. Hariharan, J.A. Pople, Theoretica Chim. Acta 28 (1973) 213.
[20] M.M. Francl, W.J. Petro, W.J. Hehre, J.S. Binkley, M.S. Gordon, D.J. DeFrees, J.A. Pople, J. Chem. Phys. 77 (1982) 3654.
[21] T. Clark, J. Chandrasekhar, R. von, P. Schleyer, J. Comp. Chem. 4 (1983) 294.
[22] R. Krishnam, J.S. Binkley, R. Seeger, J.A. Pople, J. Chem. Phys. 72 (1980) 650.
[23] P.M.W. Gill, B.G. Johnson, J.A. Pople, M. Frisch, J. Chem. Phys. Lett. 197 (1992) 499.
[24] A.P. Scott, L. Radom, J. Phys. Chem. 100 (1996) 16502.
[25] R. Krishnan, J.S. Binkley, R. Seeger, J.A. Pople, J. Chem. Phys. 72 (1980) 650.
[26] M.J. Frisch, J.A. Pople, J.S. Binkley, J. Chem. Phys. 80 (1984) 3265.
[27] C. Lee, W. Yang, R.G. Parr, Phys. Rev. B 37 (1988) 785.
[28] A.D. Becke, J. Chem. Phys. 98 (1993) 1372.
[29] A.D. Becke, J. Chem. Phys. 98 (1993) 5648.
[30] Gaussian 98 User's Reference, 2nd Edition, Gaussian Inc., 1999.
[31] P.Y. Ayala, H.B. Schlegel, J. Chem. Phys. 108 (1998) 2314 and references cited therein.
[32] S.C. Choi, R.J. Boyd, Can. J. Chem. 63 (1985) 836.

[33] S.C. Choi, R.J. Boyd, Can. J. Chem. 64 (1986) 2042.
[34] Lide, D.L. (Ed.), CRC Handbook of Chemistry and Physics, Ref. Data, 76th Edition, CRC, Boca Raton, FL, 1995.
[35] B. Bogdanov, T.B. McMahon, J. Phys. Chem. A 104 (2000) 7871.
[36] B. Bogdanov, Unpublished results, University of Waterloo.
[37] J.E. Szulejko, Unpublished results, University of Waterloo.
[38] M.A. French, S. Ikuta, P. Kebarle, Can. J. Chem. 60 (1982) 1907.
[39] G.D. Smith, R.L. Jaffe, H. Partridge, J. Phys. Chem. A 101 (1997) 1705.
[40] M. Lewis, Z. Wu, R. Glaser, J. Phys. Chem. A 104 (2000) 11355.
[41] S. Hoyau, K. Norrman, G. Ohanessian, T.B. McMahon, J. Am. Chem. Soc. 121 (1999) 8864.
[42] R. Farid, T.B. McMahon, Can. J. Chem. 58 (1980) 2307.
[43] http://webbook.nist.gov/chemistry/ion/
[44] V.F. DeTuri, M.A. Su, K.M. Ervin, J. Phys. Chem. A 103 (1999) 1468.
[45] D.A. Good, J.S. Francisco, J. Phys. Chem. A 102 (1998) 1854.
[46] A.E. de Oliveira, R.L.A. Haiduke, R.E. Bruns, Spectrochim. Acta A 56 (2000) 1329.
[47] J. Ballard, R.J. Knight, D.A. Newnham, J. Quant. Spectrosc. Radiat. Transfer 66 (2000) 199.
[48] S. Papasavva, K.H. Illinger, J.F. Kenny, J. Phys. Chem. 100 (1996) 10100.
[49] R.C. Dunbar, T.B. McMahon, D. Thöllman, D.S. Tonner, D.R. Salahub, D.J. Wei, Am. Chem. Soc. 117 (1995) 12819.
[50] J.A. Kelley, J.M. Weber, K.M. Lisle, W.H. Robertson, P. Ayotte, M.A. Johnson, Chem. Phys. Lett. 327 (2000) 1.
[51] N.L. Haworth, M.H. Smith, G.B. Bacskay, J.C. Mackie, J. Phys. Chem. A 104 (2000) 7600.